JOURNAL OF ENVIRONMENTAL SCIENCES 127 (2023) 678–687

Available online at www.sciencedirect.com

ScienceDirect

www.elsevier.com/locate/jes

JES JOURNAL OF ENVIRONMENTAL SCIENCES

www.jesc.ac.cn

Perfluoroalkyl acid transformation and mitigation by nNiFe-activated carbon nanocomposites in steady-state flow column studies

Mahsa Modiri-Gharehveran[1,**], *Younjeong Choi*[1], *Jenny E. Zenobio*[1,2,***], *Linda S. Lee*[1,2,*]

[1] *Department of Agronomy, Purdue University, West Lafayette, IN 47907, USA*
[2] *Interdisciplinary Ecological Sciences & Engineering, Purdue University, West Lafayette, IN 47907, USA*

ARTICLE INFO

Article history:
Received 19 March 2022
Revised 28 June 2022
Accepted 29 June 2022
Available online 8 July 2022

Keywords:
PFAAs
PFAS
Zero valent iron
Nanoparticles
Remediation
Groundwater

ABSTRACT

The ongoing contamination of groundwater with per- and polyfluoroalkyl substances (PFAS) has resulted in a global and rapidly growing interest in PFAS groundwater remediation. Preferred technologies that lead to PFAS destruction are often limited by not addressing all PFAS, being energy-intensive or not being suited for *in-situ* application. We developed nNiFe-activated carbon (AC) nanocomposites and demonstrated varying degrees of PFAS reduction and fluoride generation with these nanocomposites in batch reactors for several PFAS. Here we explore nNiFe-AC's effectiveness to transform perfluoroalkyl acid acids (PFAAs) under steady-state flow (0.0044 to 0.15 mL/min) in nNiFe-AC:sand packed columns. Column experiments included, two perfluorooctane sulfonate (PFOS) in deionized water and two PFAA mixtures in deionized water or bicarbonate buffer containing five perfluoroalkyl carboxylates (PFCAs, C5-C9) and three perfluoroalkyl sulfonates (PFSAs, C4, C6 and C8) at temperatures of 50 or 60°C were evaluated. PFOS transformation was similar in PFOS-only and PFAA mixture column experiments. Overall, % PFAA transformation under flow conditions exceeded what we observed previously in batch reactors with up to 53% transformation of a PFAA mixture with ~ 8% defluorination. Longer chain PFAS dominated the PFAAs transformed and a bicarbonate matrix appeared to reduce overall transformation. PFAA breakthrough was slower than predicted from only sorption due to transformation; some longer chain PFAS like PFOS did not breakthrough. Here, nNiFe-AC technology with both in-situ and ex-situ potential application was shown to be a plausible part of a treatment train needed to address the ongoing challenge for cleaning up PFAS-contaminated waters.

Introduction

Per- and polyfluoroalkyl substances (PFAS) have been found in numerous water bodies (Ahrens, 2011; Ahrens and Bundschuh, 2014) due to release from multiple uses including various industrial operations, product coatings and aqueous film forming foams (AFFFs) (Barber et al., 2017; Lau et al., 2007; Moody and Field, 2000). Perfluoroalkyl acids (PFAAs)

* Corresponding author.
E-mail: lslee@purdue.edu (L.S. Lee).
** Current address: EA Engineering, Science and Technology, Hunt Valley, MD 21031.
*** Current address: Jacobs, Irvine, CA 92612.

https://doi.org/10.1016/j.jes.2022.06.040
1001-0742/

are the most studied PFAS class and known to be persistent and the terminal metabolites of other PFAS classes (Houtz et al., 2013). PFAAs, particularly the shorter chain PFAAs (≤ 5 perfluoroalkyl carbons (Buck et al., 2011)), are quite mobile and frequently detected in groundwater (Ahrens et al., 2015; Barzen-Hanson et al., 2017; Szabo et al., 2018) which has driven concerns with groundwater being a common drinking water source (Weber et al., 2017). AFFF use (Barzen-Hanson et al., 2017; Filipiak et al., 2017; Xiao et al., 2017), landfill leachate (Lang et al., 2016), municipal wastewater discharge (Lenka et al., 2021), and wastewater reuse (Loganathan et al., 2007; Schultz et al., 2006; Sinclair and Kannan, 2006) have all been attributed to PFAS-contaminated groundwater. For example, fire-training activities using AFFF at Wurtsmith Air Force Base resulted in 3000 to 120,000 ng/L of perfluoroalkyl carboxylic acids (PFCAs) in groundwater (Moody and Field, 1999). In China, PFAAs entering groundwater from landfill leachates were estimated to be around 3110 kg/year (Yan et al., 2015). In Australia, crop irrigation using recycled water from wastewater treatment plants (WWTPs) led to PFAS detection in all groundwater samples ranging from 0.03 to 74 ng/L for a suite of 20 PFAS (Szabo et al., 2018).

To date, most of PFAS remediation techniques have been found insufficient or not cost-effective for application in practical scales (Yadav et al., 2022). Such technologies include but not limited to conventional treatment approaches such as biological degradation, oxidation, reduction, and coagulation or alternative treatments such as advanced oxidation, photocatalytic processes, anion exchange resins, adsorption and membrane technologies (Yadav et al., 2022). Such findings have led to research and investigation on potential techniques for in-situ PFAS remediation of groundwater (Xu et al., 2021).

Granular activated carbon (GAC) is commonly used to treat contaminated groundwater and drinking water above ground (McCleaf et al., 2017; Xiao et al., 2017). However, recently, in-situ colloidal AC injection into the subsurface was evaluated for mitigating groundwater concentrations of perfluorooctane sulfonate (PFOS) and perfluorooctane carboxylate (PFOA) (McGregor, 2018). A few other adsorption technologies have also been explored for in-situ use (Aly et al., 2019; Lu et al., 2020). For example, injecting cationic polymers coagulants increased PFAA adsorption capacity 2 to 6 times for C4-C8 PFAAs leading to delayed breakthrough in aquifer media packed columns and exemplifying desorption hysteresis (Aly et al., 2019). However, sorbent-only based approaches only sequester PFAS with a likelihood of re-release and the long-term liability potentially associated with spent sorbent disposition. Chemical oxidant injection into aquifers for PFAS destruction has been investigated with great expectations, but with varying results. Heat-activated persulfate oxidation was able to destroy PFCAs, but only to a limited degree before pH decreased to below 4 (Bruton and Sedlak, 2018; Park et al., 2016). Also in all in situ chemical oxidation (ISCO) tested including activated persulfate, perfluoroalkyl sulfonates (PFSAs) were not altered (Arias Espana et al., 2015; Park et al., 2020, 2016; Ross et al., 2018).

Permeable reactive barriers (PRBs) for capture and destruction of contaminated groundwater have been successful in remediation of an extensive range of contaminants (Blowes et al., 2003; Lee et al., 2009). PRBs serve as an in-situ reactive treatment zone installed perpendicular to a pollutant plume such that contaminated groundwater will flow through the reactive zone. In these systems, sorbents like activated carbon are used to immobilize or reduce pollutant transport (Kuppusamy et al., 2016) and reactive materials such as zero valent iron (Fe^0) are used to degrade pollutants (Lee et al., 2009; Tratnyek et al., 2003). In closed batch reactors, we demonstrated the use of heated (50°C) nNiFe particles supported on activated carbon (AC) to mineralize up to 94% of branched and linear PFOS isomers (100% defluorination of unrecovered PFOS) (Zenobio et al., 2020). Subsequently, transformation of several other PFCAs, PFSAs, fluorotelomer sulfonates and GenX as well as PFAA mixtures was demonstrated at 50 and 60°C (Gharehveran et al., 2021). In some cases, PFAS degradation, defluorinations, and temperature were found to be dependent on PFAS structure as well as matrix. For example, temperature effect was significant for only PFOS with doubled transformation at the lower temperature of 50 °C compared to 60 °C (Zenobio et al., 2020). So, it remains unclear how temperature effect is PFAS dependent. Preliminary efforts on mechanisms showed each of the Fe, Ni, and AC play inevitable roles in PFAS reductive transformation with highest transformation occurring for nNiFe-AC compared to ingredient variations. The role of Fe was found to be not limited to H_2 generation and the role of activated carbon to be enhancing the reactivity by preventing agglomeration and bringing PFAS closer to the reactive surface (Zenobio et al., 2020). While closed batch reactors allow for quick assessments of remediation potential and influencing parameters, potential artifacts such as the build-up of products may limit transformation yields. Here, for the first time, we quantify the effectiveness of nNiFe-AC nanocomposites to degrade and defluorinate PFAS under column flow conditions. Quantification of PFAAs and fluoride (F^-) and identification of products were monitored in both the effluents and extracts of column sections. PFAA recoveries and % defluorination between PFCAs and PFSAs as well as previously reported batch reactions are compared as well as intermediate products identified. Lastly, for this technology to be effective in a meaningfully timeframe, heat is required which is plausible given previous successful heat-based in-situ treatments such as electrical resistance heating (ERH) among other approaches (Davis, 1997).

1. Material and Methods

1.1. *Standards, Reagents, and Stock Preparation*

Sodium fluoride (NaF, 99%), sodium sulfate (Na_2SO_4, 99%), potassium perfluorooctanesulfonate (PFOSK, $C_8F_{17}SO_3K$, 98%), perfluorohexanoic acid (PFHxA, $C_5F_{11}COOH$, 98%), perfluoroheptanoic acid (PFHpA, $C_6F_{13}COOH$, 98%), perfluorooctanoic acid (PFOA, $C_7F_{15}COOH$, 98%), and heptadecafluorononanoic acid (PFNA, $C_8F_{17}COOH$, 97%) were purchased from Sigma-Aldrich (St. Louis, MO). Perfluoropentanoic acid (PFPeA, C_4F_9COOH, 98%) was obtained from Oakwood Products, Inc (Columbia, SC). Iron (II) chloride tetrahydrate ($FeCl_2.4H_2O$, 98%) was supplied by Alfa Aesar Chemicals (Ward Hill, MA). Nickel chloride hexahydrate ($NiCl_2.6H_2O$, 98%) was purchased from Honeywell (Muskegon, MI, USA).

Table 1 – Column characteristics, set-up and conditions.

	PFOS-I	PFOS-II	Mix-I	Mix-II
nNiFe-AC:sand ratio	1:10	1:10	1:10	1:7
Temperature (°C)	60	60	60	50
Influent flow (mL/min)[a]	0.05	0.15	0.036	0.0044
Influent Matrix	DI water	DI water	pH 7.5 10 mmol/L bicarbonate buffer	DI water
Effluent collection frequency (PVs)	0.6	0.8	3.2	0.4
Effluent pH mode	In-line[b]	In-line[b]	Effluent fraction[c]	Effluent fraction[c]
Effluent ORP mode	In-line[d]	NA	NA	NA
Hydraulic residence time (hr)	5.3	1.8	7.4	60
Whole column PV (mL)	16	16	16	16
Total PVs eluted	59	105	153	20
Saturated PV of reaction bed (mL)	6.8	6.8	6.8	6.1
nNiFe-AC (g, reaction bed)	4	4	4	6
Sand (g in reaction bed)	40	40	40	35
Sand (g in whole column)	85	85	85	77
ρ_b, column (g/cm^3)[e]	1.73	1.73	1.73	1.71
ρ_b, reaction bed (g/cm^3)[e]	1.56	1.56	1.56	1.40
Θ_{sat}, reaction bed (mL/cm^3)[f]	0.23	0.23	0.23	0.20
Θ_{sat}, column (Θ mL/cm^3)[f]	0.311	0.311	0.311	0.309

[a] LC pump used for all except for Mix-II which used a Harvard syringe pump;
[b] pH measured of warm effluent in-line every 10 mins for 1 day, and 180 mins for the remaining experimental period (Fig. 1);
[c] Measured in PV increments of each ~ 3.5, 3.3, and 0.35 for PFOS-I, Mix-I, and Mix-II, respectively;
[d] ORP measured in warm effluent in-line every 10 mins for 1 day, 20 mins for 8 day, and 60 mins for the remaining experimental period (Fig. 1);
[e] measured bulk density,
[f] Maximum PVs estimated using saturated volumetric water contents measured for a sand-only column (0.31 mL/cm^3) and a 1:10 spent nNiFe-AC:sand mix for whole column (0.44 mL/cm^3).

Sodium borohydride ($NaBH_4$, 99%) was obtained from ACROS Organics (Morris Plains, NJ). Activated carbon was purchased from Strem Chemicals (Newburyport, MA). Perfluoro-[^{13}C8]octanesulfonate (M8PFOS), perfluoro-n-[^{13}C8]octanoic acid (M8PFOA), and PFCA/PFSA solution/mixture (PFAC-MXB) were purchased from Wellington Laboratories (Lenexa, KS). Ammonium acetate, sodium carbonate, and sodium bicarbonate, analytical grade, were purchased from Mallinckrodt Baker, Inc (Mallinckrodt Chemicals, Phillipsburg, NJ). Acetic acid, sodium hydroxide, formic acid, and methanol were analytical grade from Fisher Scientific (Pittsburgh, PA). The N_2 gas of high purity grade (99.995%) and H_2 (4% in N_2) used for operating anaerobic chamber during the synthesis of the nanocomposites were purchased from Indiana Oxygen (Lafayette, IN). Nanopure (Thermo Scientific) water purification system was used to provide reagent grade water (≥18.2 MΩ·cm, henceforth referred to as DI water). Deoxygenated aqueous PFAA influent solutions were prepared in the anaerobic chamber (Table 1).

1.2. *Nanocomposites Synthesis*

nNiFe-AC nanocomposites were synthesized under oxygen free conditions in an anaerobic chamber as described previously (Zenobio et al., 2020). The final nanocomposite achieved was 1.7 wt% Ni, 85.5 wt% Fe, and 12.8 wt% AC. Particles were packed into columns immediately after being prepared.

1.3. *Column Characteristics and Packing*

Four column experiments (PFOS-I, PFOS-II, Mix-I and Mix-II) were conducted with variations in nNiFe-AC:sand ratios, solution matrix, flow rate, temperature and total pore volumes (PVs) eluted prior to column termination (Table 1). A Spectrum Lab glass aqueous column (2.5 cm x 10.5 cm, total inner volume of 51.5 cm^3) was packed and capped inside the anaerobic chamber before taking out to initiate flow experiments (Appendix A Table S1). For all columns, the influent end was packed with 3 cm of sand, followed by 6 cm of the nNiFe-AC:sand mix (reactive zone), and topped off with 1.5 cm of sand followed by a mesh to prevent particles from exiting the column (Fig. 1). The nNiFe-AC:sand mix reaction zone for PFOS-I, PFOS-II, and Mix-I was 1:10 whereas higher ratio of 1:7 was used for Mix-II. Autoclaved de-oxygenated nanopore water was used for the influent matrix in all columns except Mix-I which used autoclaved deoxygenated carbonate buffer (10 mmol/L; pH = 7.5). Influents were prepared to targeted concentrations (Table 2) in an anaerobic chamber by diluting aqueous stock solutions containing either PFOS or a PFAA mixture with autoclaved matrix solutions. Once packed, columns were taken out of the anaerobic chamber, appropriate polyethylene tubing attached to the columns, and columns were placed in either a water bath or wrapped with heat tape to maintain the targeted temperature (50°C for Mix-II and 60°C for the other columns, Table 1). There were not identical conditions in any two columns, thus no exact replicates; however, similarities in flow conditions and experimental temperature between PFOS-I and Mix-I serves to confirm experimental setup and reproducibility of final degradation results for PFOS as the representative PFAS.

The PFAA-containing influents were pumped through the columns in an upward constant vertical flow using either a Shimadzu LC pump for the higher flow rate or an 11-ELITE in-

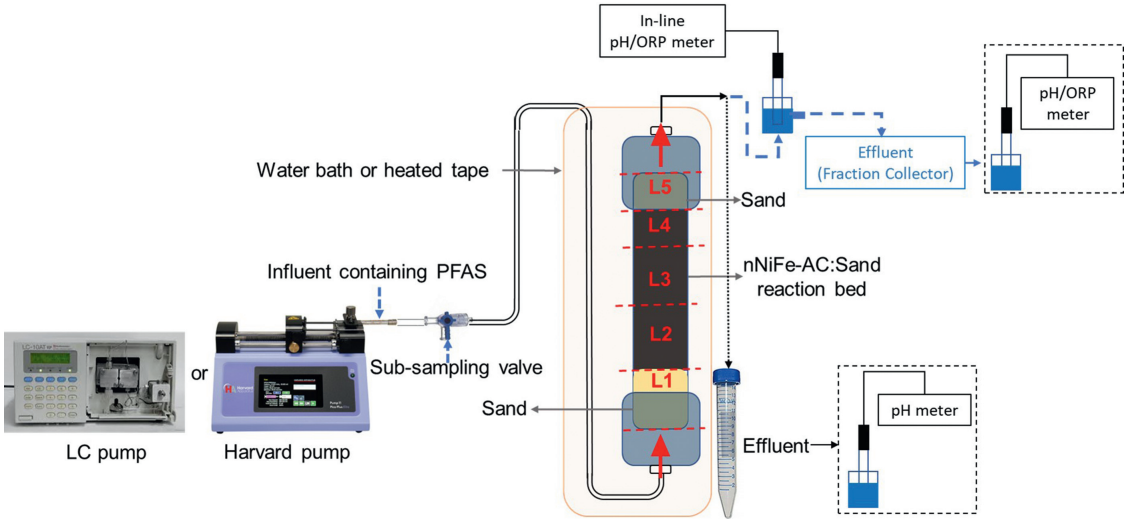

Fig. 1 – General schematic of column set ups. The details regarding individual column experiments are summarized in Table 1. L1-L5 represent column section extracted for PFAS (L2, L3, and L4 reaction bed) and F^-.

Table 2 – Average of influent concentrations of PFOS in PFOS-I and PFOS-II columns and PFAAs in Mix-I and Mix-II columns.

Compound	Concentration (ng/mL)		
	PFOS-I & -II	Mix-I*	Mix-II*
PFBS		190.4 ± 11.7	107.6 ± 10.2
PFPeA		136.1 ± 8.43	207.1 ± 16.7
PFHxA		165.3 ± 14.9	255.8 ± 22.8
PFHpA		157.2 ± 10.2	201.9 ± 14.6
PFHxS		122.5 ± 30.4	111.9 ± 9.36
PFOA		129.1 ± 20.9	179.9 ± 15.8
PFOS	2007 ± 38.8	63.90 ± 26.5	61.63 ± 5.01
PFNA		31.25 ± 11.3	165.6 ± 14.6

* The averages are for ~5 and ~30 samples corresponding to sub-sampling of freshly prepared PFAA solution, and influent left in the eluent bottle (LC pump) for Mix-I or influent left in the syringe (Harvard pump) for Mix-II, respectively.

fusion syringe pump (Harvard Apparatus, Holliston, MA, USA) for the lower flow rates (Table 1). Although influent pump rates were constant, H_2 generation from the nNiFe-AC reactions resulted in columns varying in their degrees of saturation. PVs were estimated based on saturated columns, which was not the case as reactions proceeded, therefore, PVs reported are only estimates. For Mix-I, PFAA mix solution was renewed every~20 days (total number of 3 times for 2-month period of experiment), and for Mix-II, every ~4 days (total number of ~15 times for 2-month period of experiment). Influent was sub-sampled and prepared for analysis prior to use and prior to each renewal or at the end of the experiment.

1.4. *ORP and pH Measurements*

In-line oxidation-reduction potential (ORP) measurements were made in the PFOS-I column effluent (METTLER TOLEDO, InLab Redox Micro ORP electrode) while pH was measured in all column experiments in either effluent fractions (Fisher Scientific/accumet-AR20) or in-line (Aldrich Chemical Company SO197438 pH electrode) (tabulated in Table 1). Aliquots (250 or 500 µL) from effluents collections were taken for PFAA analysis after a 5-min sonication to ensure homogeneity prior to subsampling.

1.5. *Column Processing Post Treatment*

At termination, the column and associated exit tubing were drained into pre-weighed polypropylene (PP) tubes and subsampled for PFAA analysis similar to effluents. The column bed was divided into 5 layers based on color (Appendix A Fig. S1). The first layer (influent end) was mostly sand without any nanocomposites; the second, third, and forth layers were composed of the nNiFe-AC:sand mix, and the last layer was sand containing some migrated nNiFe-AC particles. Each layer was placed in individual pre-weighed 15-mL PP tube and sub-sampled (~ 5 g wet mass) to extract for PFAS and inorganic extractions. Briefly, particles were extracted 5 times sequentially with 10 mL of acidified methanol (1% acetic acid in H_2O:MeOH 10:90 V/V) and sonication (30 min). Supernatants after centrifugation were combined into 50-mL PP tubes. For PFAS analysis, aqueous or extract supernatant aliquots were prepared with a final composition of 1:1 V/V H_2O:MeOH in 1.5-mL PP vials, spiked with appropriate isotopically mass-labeled

internal standards (ISs) and stored in the refrigerator at 4°C awaiting PFAS analysis. The inorganics were extracted 3 times sequentially with 0.02 mol/L NaOH, extracts combined in 50-mL PP tubes and stored in the refrigerator at 4°C awaiting F^- analysis.

1.6. Analytical Methods

1.6.1. PFAS Quantitation and Organic Product Identification

PFAS analysis was performed using Shimadzu ultrahigh performance liquid chromatography system (uPLC) coupled to a Sciex5600 Triple Quadrupole Time-of-Flight (QToF) mass spectrometer (MS). All samples (effluent and extracts), controls, standards, and laboratory solvent or DI water blanks were prepared to achieve a final composition of 1:1 *V/V* H_2O:MeOH with ISs in 1.5 mL PP vials. M8PFOS and M8PFOA were used as ISs for the sulfonates and carboxylates, respectively. Chromatography and MS details are detailed in the SI (Appendix A Tables S2 and S3). PFAA extraction recoveries were determined in our previous room temperature control batch reactors (tabulated in Appendix A Table S4) (Zenobio et al., 2020). Column extracts were screened for unknown byproducts using QToF/MS non-target screening as well as effluents for PFOS-I and PFOS-II following procedures described previously (Zenobio et al., 2020). Products were determined checking mass error, isotopic pattern, retention time, and identification of daughter ions corresponding to fluorine-containing fragments.

1.6.2. Inorganic Analysis with IC

The 940 Professional IC System from Metrohm with MSM II (Metrohm Suppressor Module) suppressor and conductometric detector was used for F^- analysis in the PFAS Mix columns. The PFOS only column work was done at an earlier time during which the ion chromatography column we were using was not adequately separating F- from interfering peaks. Anions were separated using Metrosep A Supp 7 (250 mm × 4 mm) from Metrohm with an 3.6 mmol/L Na_2CO_3 eluent in isocratic mode at 0.7 mL/min. The injection volume was 20 µL. The F^- limits of detection (LOD) and quantitation (LOQ) were 10 μg/L and 20 μg/L, respectively.

1.6.3. ICP-OES Analysis of Effluent for Fe and Ni

Effluents from the Mix-I and Mix-II columns were analyzed for Fe and Ni over time using a Shimadzu ICPE-9820 inductively coupled plasma optical emission spectrometer (ICP-OES) system with mini-torch technology. The auxiliary and nebulization gas flow-rates were 0.6 and 0.7 L/min, respectively. Emission lines were selected based on sensitivity where the ionic lines of Ni (221.647 nm) and Fe (259.940 nm) were measured. The LOD for Ni and Fe were 0.5 and 1 ppb, respectively.

1.7. Column Data Analysis

Individual PFAA mole recovery in column porewater, effluent and particle extracts were calculated relative to the total PFAA introduced into the column with total % recovery of all PFAAs being the sum of the individual mol % PFAA recoveries. Moles of individual PFAAs not recovered was assumed to be transformed based on previous high recoveries (Gharehveran et al., 2021) thus % net transformation calculated as moles not recovered relative to the total moles introduced. Possible PFAA loss to column walls, tubing, and fittings was also assessed. Briefly, an aqueous solution of PFOS, as a longer chain PFAA in which the highest sorption affinity is expected, at ~ 500 ng/mL was introduced into an unpacked column at ~ 0.05 mL/min for 5 days at 50°C. Subsamples of the input solution immediately after preparation, collected effluents after 5 days, and remaining solution in the feed syringe of the Harvard pump were analyzed. There were no significant differences in PFOS concentrations between the influent and effluent. Shorter chain PFAAs can be generated from longer chain PFAAs, however, the % generated relative to the initial concentrations is expected to be small on our previous batch reactor findings with similar PFAAs mixtures (Gharehveran et al., 2021). Total fluorine (F) mole balance was calculated by summing the measured F^- and PFAA-F based moles (PFAA-F: summation of fluorine atoms as $3 + 2n$ for $CF_3(CF_2)_n$-X) recovered in the effluents and extracts relative to initial PFAA-F content introduced (Eq. (1)).

$$\%\ \text{Total F mole balance} = \frac{F^-_{\text{generated}} + \text{PFAA} - F_{\text{recovered}}}{\text{PFAA} - F_{\text{in}}} \times 100\% \quad (1)$$

The % PFAA defluorination relative to the initial PFAAs (Eq. (2)) and % fluoride generated relative to the moles of transformed PFAAs (Eq. (3)) were calculated as follows:

$$\%\ \text{Defluorination relative to initial PFAA} - \text{F} = \frac{F^-_{\text{generated}}}{\text{PFAA} - F_{\text{in}}} \times 100\% \quad (2)$$

$$\%\ \text{Fluoride generated relative to transformed PFAA} - \text{F} = \frac{F^-_{\text{generated}}}{\text{PFAA} - F_{\text{transformed}}} \times 100\% \quad (3)$$

where, $\text{PFAA} - F_{\text{in}}$, and $\text{PFAA} - F_{\text{recovered}}$, and $\text{PFAA} - F_{\text{transformed}}$ are the moles of initial, recovered, and not-recovered (assumed to be transformed) PFAAs, $F^-_{\text{generated}}$ is the moles of fluoride generated; respectively.

PFAA retardation factors (*R*) were estimated (Eq. (4)) using the K_d values (L/kg) for nNiFe-AC ($K_{d,\text{ nNiFe-AC}}$) calculated from our previous batch reactor study (Gharehveran et al., 2021) after a 5-days reaction (detailed in Appendix A). Briefly, $K_{d,\text{ nNiFe-AC}}$ values from previous batch studies did not exhibit significant differences within the temperature range explored (20, 50 and 60°C); therefore, PFAA-specific K_d values averaged across temperatures were used. For the longer chain PFAAs in which aqueous concentrations were < LOQ, $K_{d,\text{nNiFe-AC}}$ values were estimated assuming a log-linear correlation with perfluorocarbon chain length using the shorter chain PFAA data. Sorption by sand ($K_{d,\text{ sand}}$) was only measured for PFOS using a 3-concentration isotherm (initial aqueous concentrations = 2, 5 and 10 ppb; Appendix A Fig. S2). For the other PFAAs, the $K_{d,\text{ sand}}$ values were estimated using the slope determined for the $K_{d,\text{ nNiFe-AC}}$ trend with shorter chain PFAAs (Appendix A Fig. S3), which showed that sorption to the sand is negligible compared to sorption by the nanocomposites (<0.3% for all PFAAs); therefore, additional isotherm measurements were not attempted. For some columns, breakthrough of some of

the longer chains did not occur during the experimental period. The reaction time for each PFAA in reaction bed was estimated using the PV of the reaction bed ($PV_{reaction\ bed}$) and the PFAA-specific retarded velocity (Eq. (5)).

$$R = 1 + (\%\ mass_{nNiFe-AC} \times K_{d,nNiFe-AC} + \%\ mass_{sand} \times K_{d,\ sand}) \frac{\rho_b}{\theta_{sat}} \quad (4)$$

$$\text{Reaction time} = \frac{PV_{reaction\ bed}}{\frac{Q_{water}}{R}} \quad (5)$$

ρ_b (g/cm^3) and θ_{sat} (mL/cm^3) are measured bulk density and saturated water content, respectively (Table 1); and Q_{water} is the actual column influent flow-rate. Attempts were made to use CXTFIT (Parker and van Genuchten, 1984) to predict PFAA breakthrough based on sorption and estimated reaction rates, but due to the transient unsaturated conditions in the columns in response to H_2 generation, the approach was not effective.

2. Results and Discussion

2.1. pH and ORP

For PFOS-I, PFOS-II and Mix-II columns with DI water-based influents, pH increased initially (first < 3 PVs) (Appendix A Fig. S4a) followed by pH decreasing consistent with our previous PFOS batch study (Zenobio et al., 2020). However, after ~ 30 PV in the highest flow rate PFOS-II column pH began to increase over time with occasionally wide fluctuations. We hypothesized that the hydroxyl ions generated upon H_2 generation in an anaerobic environment did not have time to precipitate at the higher flow rate leading to increasing effluent pH (Table 1) (Gharehveran et al., 2021; Zenobio et al., 2020). In Mix-I, which had a buffered influent (pH 7.5 bicarbonate buffer), the initial pH was low (pH 4.3 in initial PVs) but then increased to a stable plateau of 7.9 ± 0.1. For changes in ORP with time monitored only in the PFOS columns, wide fluctuations (-103 to -685 mV) in the inline ORP were observed in the first 3 PVs for the PFOS-II followed by increasing to 38 ± 10 mV. The general trend is consistent with ORP measurements made within the anaerobic glove box in our previous batch kinetic study, but in the latter, ORP values were lower (~ -800 mV at 0.5-hr reaction time and plateaued at -500 mV by ~ 1 day) (Zenobio et al., 2020). The difference may be because in-line ORP measurements were of the warm effluent.

2.2. PFAA Breakthrough Curves

For both PFOS-I (59 PVs) and PFOS-II (105 PVs), PFOS remained < LOD in the effluent. In the PFAA mix columns, PFAA breakthrough time increased with increasing chain length (Appendix A Fig. 2a), which was expected based on longer chains having higher sorption, thus retardation, and faster transformation rates (Gharehveran et al., 2021). Also higher retardation factors, translates to longer residence times in the reaction bed during which the longer chain PFAAs can transform (Langlais et al., 1991).

PFBS, PFPeA and PFHxA breakthrough occurred within ~9 PVs in both Mix columns, but breakthrough was earlier for the higher flow Mix-I (0.036 vs 0.0044 mL/min) (Fig. 2), which is likely due to nonequilibrium sorption at the higher flow (~7.4-hr hydraulic residence time) versus a 60 hr for Mix-II (Table 1). Also Mix-II had a greater mass of nanocomposites in the reaction bed, thus both sorption and transformation would have been higher (Table 1) and possibly PFAS adsorption at the air-water interface.

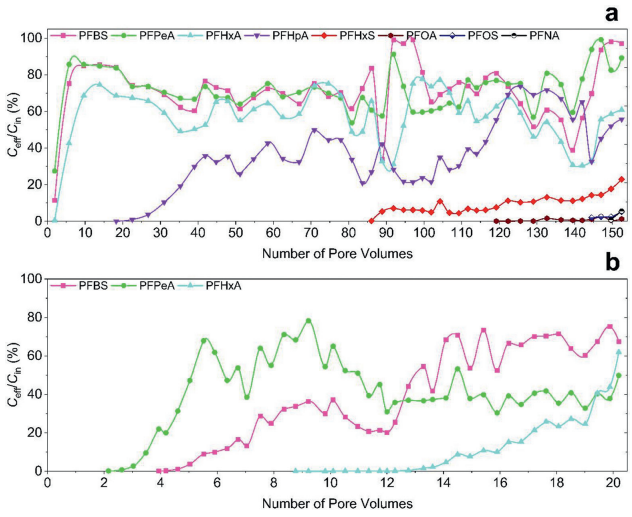

Fig. 2 – Breakthrough curves of relative concentrations for (a) Mix-I maintained at 60°C and 0.036 mL/min of PFAA-containing de-oxygenated 10 mmol/L bicarbonate buffer (pH 7.5); and (b) Mix-II maintained at 50°C and 0.0044 mL/min of PFAA-containing de-oxygenated DI water. The values inside of circle are extrapolated.

2.3. PFAA Distribution in the Column Bed at Termination

The % of individual PFAAs recovered from each column layer relative to total mass introduced is summarized in Fig. 3. Most of the PFOS mass recovered from all columns resided in layers 1 and 2 (the sand layer at the column inlet and the first layer of the reaction bed). For the other PFAAs, shorter chain PFAAs were found in layers closer to the column exit (Fig. 3b and c) as expected given their lower sorption affinity ($K_{d,PFAA}$ values, Appendix A Table S5). Differences in how the Mix columns were sectioned (Appendix A Fig. S1) resulted in the majority (≥ 50%) of the shorter chain PFAAs in layers 4 and 5 for Mix-II and layers 2 and 3 for Mix-I.

2.3. % PFAA Transformation

The total % PFAA recovered from the effluent and the column layers for all columns is plotted in Fig. 4 along with previously measured batch data for comparison. Also shown for the PFAA Mix columns is the F mole balance (F^- plus organic F from all PFAAs quantified). All unrecovered PFAS is assumed to be transformed based on 88% to 100% recovery of individual PFAAs observed previously in batch control reactors (room temperature) containing single PFAA or PFAA mixtures (Appendix A Table S4). Overall % PFAA transformation was higher in Mix-II compared to Mix-I but not % defluorination (Eq. (2)).

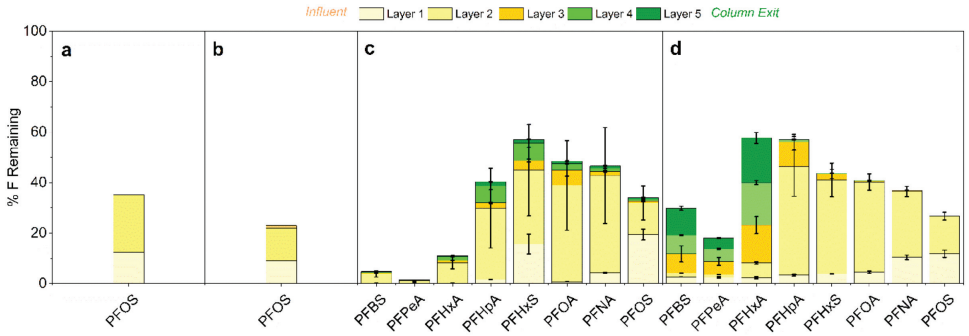

Fig. 3 – Column-layer specific PFAA moles extracted relative to total mass introduced into four different columns: (a) PFOS-I (0.05 mL/min), (b) PFOS-II (0.15 mL/min), (c) Mix-Col-I (0.036 mL/min) and (d) Mix-Col-II (0.0044 mL/min). Tabulated values summarized in Appendix A Table S6.

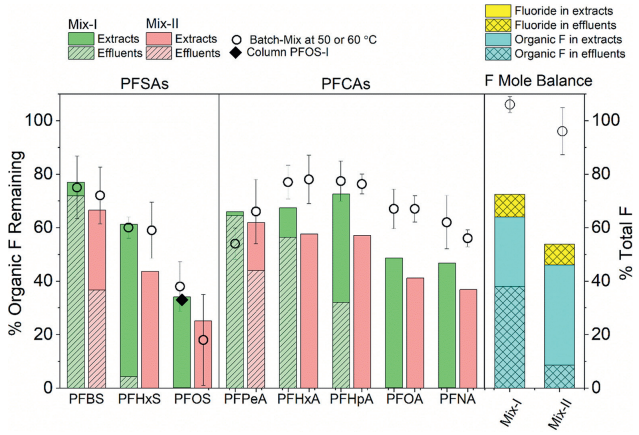

Fig. 4 – % PFAA remaining (in Mix-I and Mix -II and total F mole balance (right axis) based on organic and inorganic F recovered from the effluents and extracted from column. Column details are provided in Table 2. Symbols represent the results for batch studies at 5-days reaction period conducted at 50 or 60°C. Batch-Mix data plotted for reference are from our previous study (Gharehveran et al., 2021).

When comparing columns to batch systems at similar temperatures, generally similar % transformation was observed for PFSAs but greater transformation for PFCAs in column even with possibility of PFCAs generation from PFSAs as observed previously in batch systems (Gharehveran et al., 2021).

For PFOS, transformation was similar all 4 column studies with 65%-77% transformed (only 20%-35% recovered relative to PFOS introduced), thus not significantly impacted by three-fold difference in flow rate (PFOS-I vs PFOS-II) or the presence of other PFAAs and a bicarbonate buffer (PFOS-I vs Mix-I). In batch reactions, PFOS transformation was also similar in the presence of other PFAAs with 50% ± 6% and 62% ± 9.3% at 60°C and 94% ± 4.1% and 82% ± 17% at 50°C, in single and PFAAs mixture studies, respectively (Gharehveran et al., 2021). However, the presence of 10 mmol/L bicarbonate buffer in a PFAA mixture reaction at 50°C, decreased PFOS transformation from 82% ± 17% in DI water to 54% ± 7% in 10 mmol/L bicarbonate buffer (Gharehveran et al., 2021).

For the PFAA Mix columns, individual PFAA transformation (not recovered) ranged from 23%-73% (Fig. 4 and Appendix A Table S7). Overall total transformation of all PFAAs was higher in Mix-II (53% versus 36%) as well as between individual PFAAs (Fig. 4) with the highest increases (~43%) occurring for PFBS and PFHxS. Some of the PFCAs are both degraded and generated, thus the net change was lower (9%-24%). Mix-II had the higher nNiFe-AC mass, lower flow rate, thus longer residence times (> 22 days for all PFAAs, Appendix A Table S5), lower temperature (50°C) and the simpler matrix of DI water vs 10 mmol/L bicarbonate buffer (pH= 7.5) for Mix-I. In previous PFAA mixture batch studies (Gharehveran et al., 2021; Zenobio et al., 2020), temperature did not consistently affect all PFAAs; however, slower kinetics within a 5-days period were observed for the shorter chain PFAS, and bicarbonate buffer did reduce transformation. For both PFAA Mix columns, % transformation positively correlates to perfluorocarbon chain length with $R^2 = 0.756$ and $R^2 = 0.878$ for Mix-I (60°C, 0.036 mL/min) and Mix-II (50°C, 0.0044 mL/min), respectively (Appendix A Fig. S5) consistent with what was observed in batch reactions (Gharehveran et al., 2021). In addition to faster degradation rates for longer chain PFAAs, longer residence times also led to greater transformation for longer chain PFAAs. However, transformation (moles not recovered) under flow conditions was greater for PFAAs, particularly the PFCAs, when compared with the batch reactors.

2.4. *Total F mole balance and Organic Products*

Total F mole balance (Eq. (1)) for Mix-I and II are 73% and 55%, respectively (Appendix A Tables S8 and S9 and Fig. 4). F^- was detected in all effluent fractions for both Mix-I and Mix-II (Appendix A Fig. S6) and in the extracts of all Mix-I layers, but not in the Mix-II extracts. This is likely due to the lower mass of PFAAs introduced into Mix-II compared to Mix-I (Appendix A Tables S8 and S9) and consequently lower F^- generation leading to levels < LOD. Although % transformation was greater in Mix-II, % F^- generated from transformed PFAAs (Eq. (3)) in Mix-I (~23%) was higher than Mix-II (~14%) (Appendix A Tables S8 and S9). This led to similar overall % defluorination in both columns of ~ 8% defluorination (Eq. (2)). Much of the un-

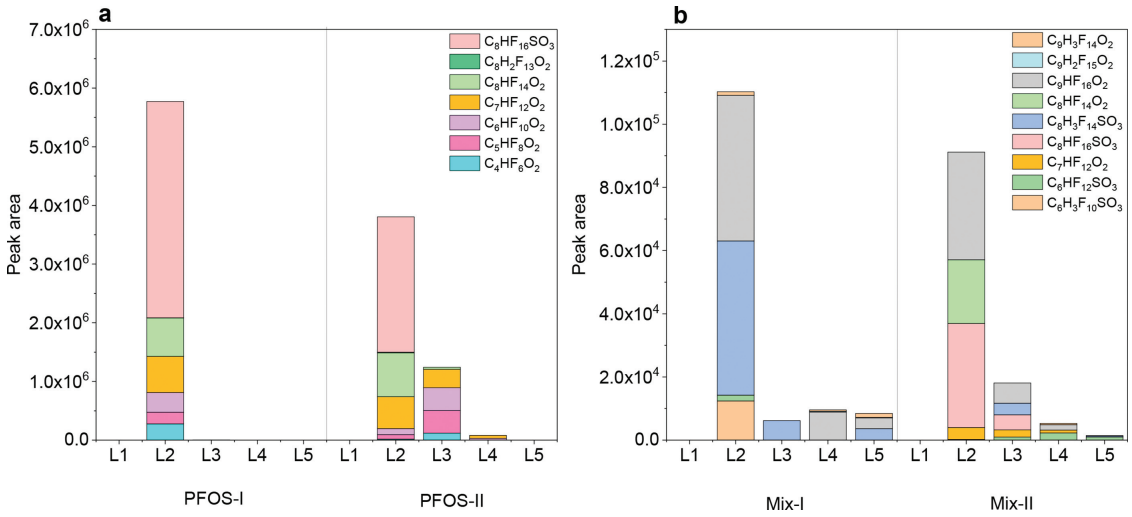

Fig. 5 – Peak areas associated with degradation products found in layers (L1-L5) of columns.

accounted F fraction may be due to unquantifiable (no standards) organic products, volatile losses of some products and potentially fluoride tightly bound to the nanocomposites.

Degradation products were identified including PFCAs, which were quantified, and numerous products from F/H exchanges or desulfonatation of PFSAs in the column layer extracts (Appendix A Tables S10 and S11, and Fig. 5) similar to those found in our previous batch studies with PFOS (Zenobio et al., 2020) and other PFAAs (Gharehveran et al., 2021). For the PFOS columns, twelve degradation products were identified including five PFCAs (PFBA, PFPeA, PFHxA, PFHpA, and PFOA), one H/F exchange ($C_8HF_{16}SO_3^-$), and six partially defluorinated desulfonated products ($C_8HF_{14}O_2^-$, $C_8H_2F_{13}O_2^-$, $C_7HF_{12}O_2^-$, $C_6HF_{10}O_2^-$, $C_5HF_8O_2^-$, and $C_4HF_6O_2^-$). For Mix-I and Mix-II, a total of nine degradation products were identified (Table S10), which included two of the ones identified in the PFOS-only columns ($C_8HF_{14}O_2^-$and $C_8H_3F_{14}SO_3$) and parallel products from PFHxS ($C_6HF_{12}SO_3^-$ and $C_6H_3F_{10}SO_3^-$) and some partially defluorinated carboxylates (e.g., $C_7HF_{12}O_2^-$, $C_9HF_{16}O_2^-$, $C_9H_2F_{15}O_2^-$, and $C_9H_3F_{14}O_2^-$). Higher peak intensities of most products were observed in the slower flow columns PFOS-I (0.05 mL/min) and Mix-I (0.036 mL/min) columns and in the first layer of the reactive zone (L2) (Fig. 5). The high number of organic products detected for just PFOS in the PFOS-I and -II columns wwere facilitated by the high PFOS mass introduced; ~30x higher PFOS compared to the PFAA mix columns (Appendix A Table S10). For PFOS-I and -II, no fluorinated intermediates were detected in the effluent even after solid phase extraction (SPE) with a 15-time concentration. For Mix-I and -II, shorter chain PFBA and perfluoropropionic acid (PFPrA) were detected in effluents (Tables S8 and 9) but accounted for < 0.1% of total F mole balance.

3. Conclusions

This study is a first step at evaluating a novel nNiFe-AC technology for PFAA treatment under steady-state flow conditions (0.04-1.42 m/day Darcy velocity) and investigates how well this technology may work in the field either as in-situ permeable reactive barriers (PRBs), above ground treatment (a reactive GAC rather than just a sorptive GAC) or in-situ injection. Although heat is required for nNiFe-AC technology, similar heat-induced remediation technologies have already been employed for remediation sites with acceptable results (Beyke and Fleming, 2005; Chien, 2012). Evaluating the appropriate in situ heating approach (e.g., ERH) and associated cost will be site-specific and dependent if other more cost-effective approaches are available. Overall, % transformation under flow conditions exceeded what we observed previously in batch reactors with up to 53% transformation of a PFAA mixture and ~ 8% defluorination of PFAAs introduced. Longer chain PFAS dominated the PFAAs transformed and a bicarbonate matrix appeared to reduce overall transformation although other parameters varied somewhat between columns. The presence of bicarbonate buffer also decreased PFOS transformation in batch studies (Gharehveran et al., 2021) which in both cases can be attributed to competition of PFAS and bicarbonate ions for reactive sites on the nanoparticle surface, thus decreasing transformation rates. Future bench-scale column studies are needed to better evaluate potential impacts of solution matrices expected in groundwater matrix including non-PFAS co-contaminants likely to be present at AFFF-impacted sites. Also, while nNiFe-AC technology may be very successful at rapidly mineralizing the longer chain PFSAs like PFOS, its use as a sole treatment step is unlikely the range of co-occurring PFAS given the differences observed across chain lengths. Therefore, nNiFe-AC nanocomposites would be best considered as part of a treatment train coupled with other treatment technologies. For example, for the PFSAs, once the sulfonate group is cleaved, attack by oxidative technologies may be more effective. Nanocomposite regeneration is also of interest especially when considering their use in PRBs. Only 0.1% to 2% of Ni and <0.01% of Fe were eluted from the column that had ~153 PVs passed through it, thus there is potential for regeneration.

Declaration of Competing Interest

The authors declare that they have no known competing financial interests or personal relationships that could have appeared to influence the work reported in this paper.

Acknowledgments

This research was funded by the Strategic Environmental Research and Development Program (No. SERDP/ER-2426), Geosyntec and the USDA National Institute of Food and Agriculture Hatch Funds Accession No. 1006516.

Appendix A Supplementary data

Supplementary material associated with this article can be found, in the online version, at doi:10.1016/j.jes.2022.06.040.

REFERENCES

Ahrens, L., 2011. Polyfluoroalkyl compounds in the aquatic environment: a review of their occurrence and fate. J. Environ. Monit. 13, 20–31. doi:10.1039/c0em00373e.

Ahrens, L., Bundschuh, M., 2014. Fate and effects of poly- and perfluoroalkyl substances in the aquatic environment: a review. Environ. Toxicol. Chem. 33, 1921–1929. doi:10.1002/etc.2663.

Ahrens, L., Norström, K., Viktor, T., Cousins, A.P., Josefsson, S., 2015. Stockholm Arlanda Airport as a source of per- and polyfluoroalkyl substances to water, sediment and fish. Chemosphere 129, 33–38. doi:10.1016/j.chemosphere.2014.03.136.

Aly, Y.H., McInnis, D.P., Lombardo, S.M., Arnold, W.A., Pennell, K.D., Hatton, J., et al., 2019. Enhanced adsorption of perfluoro alkyl substances for in situ remediation. Environ. Sci. Water Res. Technol. 5, 1867–1875. doi:10.1039/C9EW00426B.

Arias Espana, V.A., Mallavarapu, M., Naidu, R., 2015. Treatment technologies for aqueous perfluorooctanesulfonate (PFOS) and perfluorooctanoate (PFOA): A critical review with an emphasis on field testing. Environ. Technol. Innov. 4, 168–181. doi:10.1016/j.eti.2015.06.001.

Barber, L.B., Weber, A.K., LeBlanc, D.R., Hull, R.B., Sunderland, E.M., Vecitis, C.D., 2017. Poly- and perfluoroalkyl substances in contaminated groundwater. Cape Cod, Massachusetts, 2014-2015 (ver. 1.1, March, 2017) U.S. Geological Survey data release.

Barzen-Hanson, K.A., Roberts, S.C., Choyke, S., Oetjen, K., McAlees, A., Riddell, N., et al., 2017. Discovery of 40 classes of Per- and Polyfluoroalkyl substances in historical aqueous film-forming foams (AFFFs) and AFFF-impacted groundwater. Environ. Sci. Technol. 51, 2047–2057. doi:10.1021/acs.est.6b05843.

Beyke, G., Fleming, D., 2005. In situ thermal remediation of DNAPL and LNAPL using electrical resistance heating. Remediat. J. 15, 5–22. doi:10.1002/rem.20047.

Blowes, D.W., Ptacek, C.J., Jambor, J.L., Weisener, C.G., 2003. 9.05 - The Geochemistry of Acid Mine Drainage. In: Holland, H.D., Turekian, K.K. (Eds.), Treatise on Geochemistry. Pergamon, Oxford, pp. 149–204. doi:10.1016/B0-08-043751-6/09137-4.

Bruton, T.A., Sedlak, D.L., 2018. Treatment of perfluoroalkyl acids by heat-activated persulfate under conditions representative of in situ chemical oxidation. Chemosphere 206, 457–464. doi:10.1016/j.chemosphere.2018.04.128.

Buck, R.C., Franklin, J., Berger, U., Conder, J.M., Cousins, I.T., de Voogt, P., et al., 2011. Perfluoroalkyl and polyfluoroalkyl substances in the environment: terminology, classification, and origins. Integr. Environ. Assess. Manag. 7, 513–541. doi:10.1002/ieam.258.

Chien, Y.-C., 2012. Field study of in situ remediation of petroleum hydrocarbon contaminated soil on site using microwave energy. J. Hazard. Mater. 199–200, 457–461. doi:10.1016/j.jhazmat.2011.11.012.

E.L. Davis, 1997. How heat can enhance in-situ soil and aquifer remediation: important chemical properties and guidance on choosing the appropriate technique.

Filipiak, P., Bobrowski, K., Hug, G.L., Pogocki, D., Schöneich, C., Marciniak, B., 2017. New insights into the reaction paths of 4-Carboxybenzophenone triplet with oligopeptides containing N- and C-Terminal methionine residues. J. Phys. Chem. B 121, 5247–5258. doi:10.1021/acs.jpcb.7b01119.

Gharehveran, M.M., Zenobio, J.E., Lee, L.S., 2021. Transformation and defluorination by nNiFe-activated carbon nanocomposites: PFAS structure and matrix effects. J. Environ. Chem. Eng. 9, 106901. doi:10.1016/j.jece.2021.106901.

Houtz, E.F., Higgins, C.P., Field, J.A., Sedlak, D.L., 2013. Persistence of perfluoroalkyl acid precursors in AFFF-impacted groundwater and soil. Environ. Sci. Technol. 47, 8187–8195. doi:10.1021/es4018877.

Kuppusamy, S., Palanisami, T., Megharaj, M., Venkateswarlu, K., Naidu, R., 2016. In: de Voogt, P. (Ed.), In-Situ Remediation Approaches for the Management of Contaminated Sites: A Comprehensive Overview BT - Reviews of Environmental Contamination and Toxicology Volume 236. Springer International Publishing, Cham, pp. 1–115. doi:10.1007/978-3-319-20013-2_1.

Lang, J.R., Allred, B.M., Peaslee, G.F., Field, J.A., Barlaz, M.A., 2016. Release of Per- and Polyfluoroalkyl Substances (PFASs) from carpet and clothing in model anaerobic landfill reactors. Environ. Sci. Technol. 50, 5024–5032. doi:10.1021/acs.est.5b06237.

Langlais, B., Reckhow, D.A., Brink, D.R., 1991. Ozone in Water Treatment. Lewis Publishers, Boca Raton, FL.

Lau, C., Anitole, K., Hodes, C., Lai, D., Pfahles-Hutchens, A., Seed, J., 2007. Perfluoroalkyl acids: a review of monitoring and toxicological findings. Toxicol. Sci. 99, 366–394. doi:10.1093/toxsci/kfm128.

Lee, K.-J., Lee, Y., Yoon, J., Kamala-Kannan, S., Park, S.-M., Oh, B.-T., 2009. Assessment of zero-valent iron as a permeable reactive barrier for long-term removal of arsenic compounds from synthetic water. Environ. Technol. 30, 1425–1434. doi:10.1080/09593330903186240.

Lenka, Swadhina Priyadarshini, Kah, Melanie, Padhye, Lokesh P, 2021. A review of the occurrence, transformation, and removal of poly- and perfluoroalkyl substances (PFAS) in wastewater treatment plants. Water Research 199, 117187. doi:10.1016/j.watres.2021.117187.

Loganathan, B.G., Sajwan, K.S., Sinclair, E., Senthil Kumar, K., Kannan, K., 2007. Perfluoroalkyl sulfonates and perfluorocarboxylates in two wastewater treatment facilities in Kentucky and Georgia. Water Res 41, 4611–4620. doi:10.1016/j.watres.2007.06.045.

Lu, D., Sha, S., Luo, J., Huang, Z., Zhang Jackie, X., 2020. Treatment train approaches for the remediation of per- and polyfluoroalkyl substances (PFAS): A critical review. J. Hazard. Mater. 386, 121963. doi:10.1016/j.jhazmat.2019.121963.

McCleaf, P., Englund, S., Östlund, A., Lindegren, K., Wiberg, K., Ahrens, L., 2017. Removal efficiency of multiple poly- and

perfluoroalkyl substances (PFASs) in drinking water using granular activated carbon (GAC) and anion exchange (AE) column tests. Water Res 120, 77–87. doi:10.1016/j.watres.2017.04.057.
McGregor, R., 2018. Situ treatment of PFAS-impacted groundwater using colloidal activated Carbon. Remediat. J. 28, 33–41. doi:10.1002/rem.21558.
Moody, C.A., Field, J.A., 2000. Perfluorinated surfactants and the environmental implications of their use in fire-fighting foams. Environ. Sci. Technol. 34, 3864–3870. doi:10.1021/es991359u.
Moody, C.A., Field, J.A., 1999. Determination of perfluorocarboxylates in groundwater impacted by fire-fighting activity. Environ. Sci. Technol. 33, 2800–2806. doi:10.1021/es981355.
Park, S., Lee, L.S., Medina, V.F., Zull, A., Waisner, S., 2016. Heat-activated persulfate oxidation of PFOA, 6:2 fluorotelomer sulfonate, and PFOS under conditions suitable for in-situ groundwater remediation. Chemosphere 145, 376–383. doi:10.1016/j.chemosphere.2015.11.097.
Park, S., Lee, L.S., Ross, I., Hurst, J., 2020. Evaluating perfluorooctanesulfonate oxidation in permanganate systems. Environ. Sci. Pollut. Res. Int. 27, 13976–13984. doi:10.1007/s11356-020-07803-7.
Parker, J.C., van Genuchten, M.T., 1984. Determining transport parameters from laboratory and field tracer experiments. Virginia Agricultural Experiment Station Bulletin 84-3.
Ross, I., McDonough, J., Miles, J., Storch, P., Thelakkat Kochunarayanan, P., Kalve, E., et al., 2018. A review of emerging technologies for remediation of PFASs. Remediat. J. 28, 101–126. doi:10.1002/rem.21553.
Schultz, M.M., Higgins, C.P., Huset, C.A., Luthy, R.G., Barofsky, D.F., Field, J.A., 2006. Fluorochemical mass flows in a municipal wastewater treatment facility. Environ. Sci. Technol. 40, 7350–7357. doi:10.1021/es061025m.
Sinclair, E., Kannan, K., 2006. Mass loading and fate of perfluoroalkyl surfactants in wastewater treatment plants. Environ. Sci. Technol. 40, 1408–1414. doi:10.1021/es051798v.
Szabo, D., Coggan, T.L., Robson, T.C., Currell, M., Clarke, B.O., 2018. Investigating recycled water use as a diffuse source of per- and polyfluoroalkyl substances (PFASs) to groundwater in Melbourne. Australia. Sci. Total Environ. 644, 1409–1417. doi:10.1016/j.scitotenv.2018.07.048.
Tratnyek, P., Scherer, M., Johnson, T., Matheson, L., 2003. Permeable reactive barriers of iron and other zero-valent metals. Environ. Sci. Pollut. Control Ser. 26, 371–421.
Weber, A.K., Barber, L.B., LeBlanc, D.R., Sunderland, E.M., Vecitis, C.D., 2017. Geochemical and hydrologic factors controlling subsurface transport of poly- and perfluoroalkyl substances. Cape Cod, Massachusetts. Environ. Sci. Technol. 51, 4269–4279. doi:10.1021/acs.est.6b05573.
Xiao, X., Ulrich, B.A., Chen, B., Higgins, C.P., 2017. Sorption of Poly- and Perfluoroalkyl Substances (PFASs) Relevant to Aqueous Film-Forming Foam (AFFF)-impacted groundwater by biochars and activated carbon. Environ. Sci. Technol. 51, 6342–6351. doi:10.1021/acs.est.7b00970.
Xu, B., Liu, S., Zhou, J.L., Zheng, C., Weifeng, J., Chen, B., et al., 2021. PFAS and their substitutes in groundwater: Occurrence, transformation and remediation. J. Hazard. Mater. 412, 125159. doi:10.1016/j.jhazmat.2021.125159.
Yadav, S., Ibrar, I., Al-Juboori, R.A., Singh, L., Ganbat, N., Kazwini, T., et al., 2022. Updated review on emerging technologies for PFAS contaminated water treatment. Chem. Eng. Res. Des. 182, 667–700. doi:10.1016/j.cherd.2022.04.009.
Yan, H., Cousins, I.T., Zhang, C., Zhou, Q., 2015. Perfluoroalkyl acids in municipal landfill leachates from China: Occurrence, fate during leachate treatment and potential impact on groundwater. Sci. Total Environ. 524–525, 23–31. doi:10.1016/j.scitotenv.2015.03.111.
Zenobio, J.E., Modiri-Gharehveran, M., Perre, Chloe, deVecitis, C.D., Lee, L.S., 2020. Reductive Transformation of Perfluorooctanesulfonate by nNiFe0-Activated Carbon. J. Hazard. Mater. 397, 122782. doi:10.1016/j.jhazmat.2020.122782.